chemosensors

Article

Electrochemical Detection of Dopamine with Graphene Oxide Carbon Dots Modified Electrodes

Omar Isaac Torres-Soto [1], Alejandro Vega-Rios [1], Rocio B. Dominguez [2,*] and Velia Osuna [2,*]

[1] Centro de Investigación en Materiales Avanzados, S.C. (CIMAV), Miguel de Cervantes #120, Complejo Industrial Chihuahua, Chihuahua 31136, Mexico; omar.torres@cimav.edu.mx (O.I.T.-S.); alejandro.vega@cimav.edu.mx (A.V.-R.)
[2] CONAHCyT-CIMAV, Miguel de Cervantes #120, Complejo Industrial Chihuahua, Chihuahua 31136, Mexico
* Correspondence: berenice.dominguez@cimav.edu.mx (R.B.D.); velia.osuna@cimav.edu.mx (V.O.); Tel.: +52-614-439-4832 (V.O.)

Abstract: In this work, the influence of surface functionalization due to synthesis conditions of graphene oxide quantum dots GOQDs was evaluated for dopamine (DA) detection. GOQDs were synthesized using HNO_3 (6 M or 8 M) through a liquid-phase oxidation method. The characterization (HRTEM, FTIR, Raman, and XRD) and evaluation by amperometry (AMP) and differential pulse voltammetry (DPV) showed that GOQDs-8 synthesized with higher oxygen content were more sensitive and selective in DA detection than GOQDs-6. The synergistic effects of electrostatic attraction from glassy carbon electrode negatively charged surface, functionalization for inner-sphere mechanism, and edge effect from lower particle size resulted in amplified electrochemical signal achieving detection at nanomolar level using AMP and DPV. When evaluated using AMP, GCE/GOQDs-8 showed a sensitivity of 0.0422 μA μM^{-1}, a limit of detection (LOD) of 17.6 nM, a linear range from 0.1 to 100 μM, and minimal interference for uric acid, levodopa, and acetaminophen. In contrast, using DPV, the GCE/GOQDs-8 exhibited a sensitivity of 0.0616 μA μM^{-1}, a LOD of 506 nM, and a linear range from 0.1–30 μM with remarkable selectivity from all interferent species. The assay of GOQDs-8/GCE sensor in normal human serum proved to be feasible for the practical determination of DA. The recovery obtained was in the range of 94.1 to 112.8% with a relative standard deviation (RSD), n = 3 of less than 3.62%. The oxygen-rich material showed a promising performance that can be further improved with additional nanocarbon or conducting polymers supports.

Keywords: dopamine; electrochemical sensor; graphene oxide quantum dots; oxygen functionalization

check for updates

Received: 6 November 2024
Revised: 28 December 2024
Accepted: 30 December 2024
Published: 3 January 2025

Citation: Torres-Soto, O.I.; Vega-Rios, A.; Dominguez, R.B.; Osuna, V. Electrochemical Detection of Dopamine with Graphene Oxide Carbon Dots Modified Electrodes. *Chemosensors* **2025**, *13*, 7. https://doi.org/10.3390/chemosensors13010007

Copyright: © 2025 by the authors. Licensee MDPI, Basel, Switzerland. This article is an open access article distributed under the terms and conditions of the Creative Commons Attribution (CC BY) license (https://creativecommons.org/licenses/by/4.0/).

1. Introduction

Dopamine (DA) is a catecholaminergic neurotransmitter synthesized in the central peripheral nervous system [1]. It is a monoamine consisting of a catechol ring and an ethylamine side chain. It plays a significant role in the synaptic plasticity mechanism and is involved in neuromodulation, motor control, cognitive function, regulation of various metabolic processes, hormonal balance, and the renal system. Therefore, dysregulation of normal dopamine levels has been associated with some physical and neurodegenerative diseases such as Alzheimer's [2], Parkinson's, dementia, drug addiction, depression, and schizophrenia, and neurodevelopmental disorders such as autism and attention deficit hyperactivity disorder [3,4]. The use of DA as a biomarker is of relevant importance in the clinical diagnosis of various disorders and diseases related to the nervous system, and this

will allow the pharmacological and therapeutic approach in the early stages of the diseases, increasing the quality of life of patients.

Early investigations in electrochemical studies demonstrated that the catecholamines were susceptible to oxidization, generating $2e^-$ and $2H^+$ [5,6]. Notably, DA can be oxidized to *o*-dopamine quinone (DQ) by electrochemical methods in a multi-step mechanism involving several reaction intermediates [7,8]. In fact, the first electrodes for DA sensing were carbon paste microelectrodes [9,10], carbon fiber microelectrodes [11,12], and glassy carbon electrode (GCE) [13]. Currently, carbon-based nanomaterials, including graphene and its derivates, carbon nanotubes, and other allotropes, with differences in the C/O content, electrocatalytic activity, surface defects, and the abundance of oxygen containing functional groups have shown significant influence in the selectivity and sensitivity towards DA [7,8,14,15].

Graphene oxide quantum dots (GOQDs) are zero-dimensional graphene nanoparticles derived from graphene oxide (GO), which have oxygenated functional groups at their surface [16]. GOQDS have attracted extensive attention in different areas, e.g., medicine and environmental remediation, because GOQDs are carbon-based, enhanced activity, relatively easy synthesis, low toxicity, high solubility, chemical stability, and photoluminescent properties [17]. Several research groups have reported GOQDs synthesizing through a liquid-phase oxidation reaction approach with nitric acid (HNO_3) using GO as a precursor [18–22]. In these methodologies, GOQDs of around 3 to 5 nm have been obtained, with enhanced optical properties linked to the high concentration of oxygen and nitrogen atoms on the surface. Hence, functionalization can influence the final properties of the resulting GOQDs and the sensing properties overall.

GOQDs have several advantages, including tunable band gap, high water solubility, and easy surface functionalization due to the content of multiple functional groups on their surface [23]. Furthermore, GOQDs possess various electrochemical properties that allow them to be materials with high potential as transducers, such as heterogeneous electron transfer, high current density, and high conductivity due to quantum confinement and edge effect [24]. Biosensors can benefit from their use as platforms because GOQDs can interact with various molecules through active sites like π-π electrostatic and covalent interactions [24]. For instance, Li et al. reported the functionalization of GOQDs through self-assembly monolayers with ethylenediamine for sensitive DA detection. In addition, they found that the electrochemical detection towards DA was enhanced by modifying its surface with GQDs–ethylenediamine, obtaining a linear detection range and a LOD of 1 to 150 μM and 0.115 μM, respectively [25].

Moreover, Zheng et al. modified a GCE with oxygen-rich functionalized GQDs for the electrochemical detection of DA at a pH of 7.0 in a phosphate buffer solution (0.1 M). They found that surface functionalization of GQDs with carboxylate groups generated an electrostatic interaction towards DA [26]. Likewise, Chen et al. reported the preparation of a GQD from polyacrylonitrile-based carbon fibers for the electrochemical oxidation of DA. The as-synthesized GQDs also showed high catalytic activity in DA oxidation and a linear range detection towards DA of 1–300 μM [27]. Thadathil et al. fabricated a N-GQDs/GCE in situ N-Doping that enhanced the sensitive and selective electrochemical response towards the electrochemical detection of DA within the linear ranges of 0.001–1000 μM and a LOD of 0.2 and 0.15 nM [28].

Despite these works, few studies of GOQDs from GO obtained by the Hummers method as an electrochemical sensor for DA detection have been explored. Furthermore, the effect of HNO_3 concentration on GOQDs surface, particularly the generation of the carboxylic acid group and its evaluation as an electrochemical sensor for DA at a pH of 7.4 in phosphate buffer solution, has hardly ever been studied.

In this work, we evaluate the influence of surface functionalization of GOQDs due to synthesis conditions in the final electrochemical detection of DA by amperometry and differential pulse voltammetry. GOQDs were synthesized through a liquid-phase oxidation reaction with HNO_3 (6 or 8 M) using GO as a precursor. The materials were characterized and applied to modify the surface of a GCE that was subsequently evaluated as an electrochemical sensor for DA solutions. The results showed that oxygen-rich groups in GOQDs of lower size (around 2.5 nm) correlated well with sensitive and selective DA detection at the nanomolar level.

2. Materials and Methods

2.1. Materials and Reagents

Graphite flakes (325 mesh, 99.8% (metal basis), supplied by Alfa Aesar. Sodium nitrate (99%, Fermont, Monterrey, Mexico), potassium permanganate (99.2%, Fermont, Monterrey, Mexico), sulfuric acid (96.2% *w*/*w* ACS grade by Fisher Scientific), nitric acid (70% *w*/*w* ACS grade, Fermont, Monterrey, Mexico), sodium hydroxide (Fermont, Monterrey, Mexico), hydrogen peroxide (30% Golden Bell, Anaheim, CA, USA). The reagents sodium phosphate dibasic (Na_2HPO_4), potassium phosphate monobasic (KH_2PO_4), dopamine, uric acid, ascorbic acid, acetaminophen, levodopa, and potassium chloride (KCl), normal human serum (NHS) were purchased from Sigma-Aldrich (St. Louis, MO, USA). Tri-distilled water (J.T.Baker, Chihuahua, Mexico) was used throughout all the experiments. After each measurement, an electrode polishing kit (Allum, Orlando, FL, USA) was used for surface renewal.

2.2. Synthesis of GOQDs

GO was obtained employing a modified Hummers method [29]. GOQDs were synthesized according to a previously reported procedure [18]. Firstly, tri-distilled water was used to reduce ion contamination during synthesis and sensor evaluation. In order to prepare GOQDs, 0.3 g of GO was put into a 300 mL round bottom flask placed in an oil bath. Then, after adding 150 mL of HNO_3 (6 or 8 M) into the flask, it was refluxed for 12 h at 110 °C. The solution was then cooled to room temperature and dispersed with distilled water. Subsequently, the product was neutralized at a pH close to 7 with 50 mL of NH_4OH (0.1 M), according to the Dong et al. procedure [18]. The supernatant was dialyzed using a 14 kDa cellulose membrane for approximately 48 h, with tri-distilled water replaced every 6 h until the water became clear. Then, the solid residue was diluted and sonicated for 30 min. Finally, the resulting product was dried at 60 °C for 24 h, obtaining GOQDs with different oxidation degrees. GOQDs samples were marked as GOQDs-6 and GOQDs-8, respectively, according to the concentration of HNO_3 utilized.

2.3. Sensor Fabrication

Before material deposition, the glassy carbon electrode (GCE) was polished with diamond solution (1 µm, Allum, USA) and alumina solution (0.05 µm, Allum, USA). Briefly, the polishing technique consists of an infinite or eight movement shape of the GCE over the diamond pad surface and, similarly, for the alumina pad until the GCE surface is mirror-shinny [30]. Afterward, ultrasonicated in deionized water and methanol (%*v*/*v* = 1:1) for 5 min was applied to the working electrode recently polished. To prepare the modified electrode, 1 mg of either GOQDs-6 or GOQDs-8 was dispersed in 1 mL of deionized water by sonicating in an ultrasonic bath for 1 h. Then, 10 µL of GOQDs-6 or GOQDs-8 (1 mg/mL) was drop-casted onto the GCE surface and let dry at room temperature, resulting in GOQDs-6/GCE or GOQDs-8/GCE. Finally, the modified electrode was dried at room temperature. The working electrode was polished once the measurement was done.

2.4. Characterization

The GOQDs-6 and GOQDs-8 were characterized by XRD, FTIR, RAMAN, HRTEM, and electrochemical measurements. Likewise, graphite and GO as blanks were analyzed. X-ray diffraction analysis was conducted with a PANAlytical X-pert pro (Almelo, The Netherlands) with a Cu-Kα radiation source (λ = 1.54 Å) and a 2θ between 4° and 40° with a step size of 0.05° and a time step of 0.8 s. FT-IR analysis was measured using an IR Affinitiy 1S spectrometer (Shimadzu, Kyoto, Japan). Spectra were obtained by reflectance employing a Total Attenuated Reflectance accessory. The samples were analyzed in transmittance mode in the range from 400 cm^{-1} to 4000 cm^{-1}. Raman spectroscopy analysis was performed on a LabRAM HR Evolution (Horiba Jobin Yvon, Longjumeau, France). Raman spectra were analyzed in the range of 500 cm^{-1}–2500 cm^{-1} at room temperature with a 632.8 mm He-Ne laser. High-resolution micrographs were obtained by High-Resolution Transmission Electron Microscopy (HRTEM) (TEM JEM-2200FS+CS, JEOL, Tokyo, Japan) at 200 kV.

2.4.1. Electrochemical Measurements

The electrochemical properties of the GOQDs-6/GCE or GOQDs-8/GCE were studied by cyclic voltammetry (CV), amperometry (AMP), and differential pulse voltammetry (DPV). The electrochemical techniques were performed utilizing a potentiostat/galvanostat/FRA Squidstat™ Plus electrochemical workstation (Admiral Instruments, AZ, USA) coupled with a conventional three-electrode cell. The reference electrode was Ag/AgCl, the counter-electrode was a platinum wire, and the working electrode was either GOQDs-6/GCE or GOQDs-8/GCE sensor. For every experiment, 1X phosphate buffer solution (PBS) (pH = 7.4) was utilized as the electrolyte. CV measurements were conducted by cycling the potential from –0.2 to +0.8 V (vs. Ag/AgCl) at a scan rate from 5 to 100 mV/s, containing 50 μM of DA. The conditions for the amperometry experiments were as follows: the potential of a working electrode is stepped at 0.18 V regarding reference electrode Ag/AgCl with a stabilization time of 120 s and DA addition every 60 s. The sampling interval was 0.5 s. The DPV technique was obtained with a pulse amplitude of 10 mV, pulse width of 0.05 s, pulse period of 0.2 s, scan rate of 5 mV/s, a potential step of 5 mV, quiet time of 5 s, and window potential from –0.5 to 0.5 V. The evaluated concentration range in DPV was 0.1 to 100 μM of DA.

The selectivity of GOQDs-6/GCE and GOQD-8/GCE sensors was evaluated in the presence of interferent species such as uric acid (UA), ascorbic acid (AA), acetaminophen (AC), and levodopa (L-DOPA) utilizing the same experimental conditions of AMP and DPV for DA detection. The interference concentrations were 10 μM for all substances.

2.4.2. Assay of DA in Normal Human Serum

To evaluate the practical feasibility of GOQD-8/GCE, the detection of DA in normal human serum (NHS) by DPV was carried out. The NHS was diluted 150 times with 1X PBS (pH = 7.4) before measurement. The recoveries were used with 10 concentrations of DA from 0.55 μM to 50 μM.

3. Results and Discussion

3.1. X-Ray Diffraction, FTIR, and Raman Spectroscopy

In order to validate the crystallographic results of the synthesized materials, the XRD patterns of graphite, GO, GOQDs-6, and GOQDs-8 were obtained, see Figure 1a–d), respectively. Graphite presents a strong diffraction peak at around $2\theta \approx 26.5°$ corresponding to the plane 002, see Figure 1a. The interplanar distance of 0.34 nm represents the organized layered structure of graphite [31]. On the other hand, GO exhibits a signal at around $2\theta \approx 11.7°$ corresponding to the plane 001, see Figure 1b. The interlayer spacing increased

to 0.75 nm due to changes between sp^2 to sp^3 carbon orbitals, according to the results reported by Krishnamoorthy et al. [32]. Likewise, the XRD pattern of GOQDs-6 displays a broad and low-intensity signal close to $2\theta \approx 12.7^\circ$, indicating the reduction of oxygen functional groups, see Figure 1c.

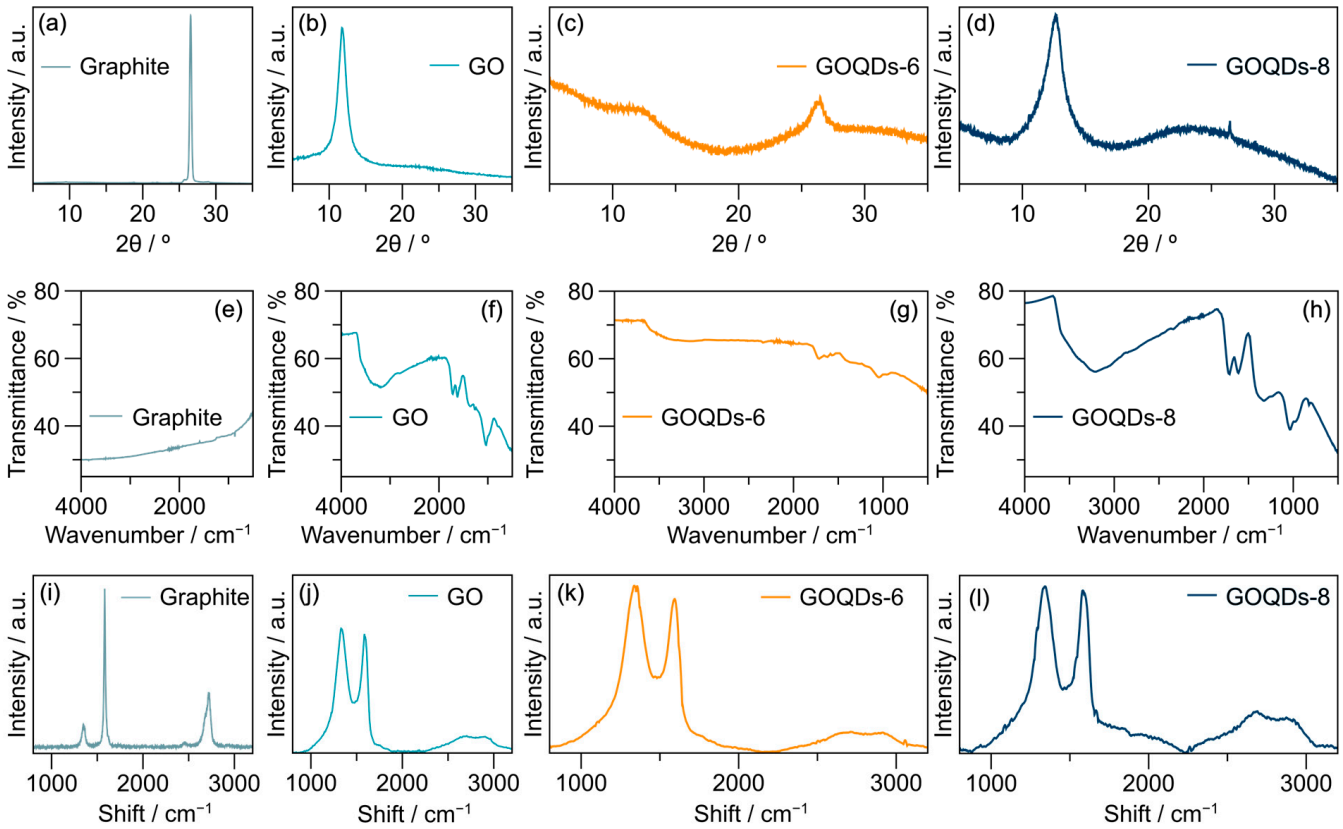


Figure 1. (**a**–**d**) XRD patterns of graphite (gray), graphene oxide (GO) line turquoise, graphene oxide quantum dots synthetized with HNO_3 (6 M) (GOQDs-6) line deep blue and graphene oxide quantum dots synthetized with HNO_3 (8 M) (GOQDs-8) line orange, respectively. (**e**–**h**) FTIR spectra of graphite, GO, GOQDs-6, and GOQDs-8, respectively. (**i**–**l**) Raman spectra of graphite, GO, GOQDs-6, and GOQDs-8, respectively.

Furthermore, the GOQDs-6 exhibits a signal centered at $2\theta \approx 26.4^\circ$ that indicates the formation of GOQDs [18]. This finding can be explained by the fact that the GO being exposed to HNO_3, the interlayer spacing decreased to 0.35 nm, indicating that graphene layers present a few disordered stacking structures as a result of surface functionalization with OH and COOH groups [33]. In the same way, the broad signal at around $2\theta \approx 26.5^\circ$ indicates that the graphitic crystalline lattice of GOQDs is functionalized and organized into graphene oxide layers [34]. Regarding the GOQDs-8 diffraction pattern, it displays a peak close to $2\theta \approx 12.7^\circ$, which is more prominent and intense than that observed in GOQDs-6, suggesting that more oxygen groups were added at the edges, see Figure 1d. Ahirwar et al. [35] reported a peak in the diffraction pattern at 9° for GQDs/GOQDs (synthesized by the electrochemical exfoliation method) owing to the presence of the oxygen-rich functional group. Lastly, the average diameter of the crystallite size was calculated by the Debye-Scherrer [36] and was around ≈1.25 and ≈1.22 nm for GOQDs-6 and GOQDs-8, respectively. This decrement in the crystallite size on GOQDs-8 is attributed to the nanometric nature of the GOQDs.

FTIR was utilized to identify the functional groups that exist in graphite, GO, GOQDs-6, and GOQDS-8, see Figure 1e–h, respectively. Figure 1f–h displays the characteristic

peaks corresponding to –OH, C=O, C=C, and C–O–C groups close to 3400, 1720, 1620, and 1040 cm^{-1}, respectively. Compared to the GO spectrum (Figure 1f), the GOQDs-6 (Figure 1g) and GOQDs-8 (Figure 1h) spectra also exhibit the stretching vibration and deformation vibration of the alcohol hydroxyl group at 3400 and 1040 cm^{-1}, respectively, due to a significant dehydration reaction between GO and HNO_3 [37]. It is worth noting the appearance of two weak peaks in the C–H stretching region of the alkanes, specifically at 2846 and 2920 cm^{-1} for the GOQDs-8 [38]. Likewise, Shao et al. [19] reported increased C–H stretching vibration for GQDs when employing HNO_3 (14.6 M). In contrast, Zhiqiang Chen et al. [37] reported that the stretching vibrations assigned to methylene and methoxy disappeared with increasing HNO_3 for alkali lignin-based carbon dots. They suggest that the strongly acidic environment may lead to C–H bond breaking and remodeling of the aliphatic groups in the side chain of the benzene ring [37].

Raman spectroscopy is a powerful analytical technique used to obtain the structural characterization of graphitic materials. Generally, these materials exhibit a graphitic band (G-band) and disorder (D-band) [39]. Figure 1i–l displays the Raman spectra obtained for graphite, GO, GOQDs-6, and GOQDs-8, respectively. Graphite spectra (Figure 1i) display a weak D signal at 1348 cm^{-1} corresponding to a graphitic lattice vibration mode, a strong G band at 1581 cm^{-1} corresponding to the sp^2 in-plane carbon atoms, and a slightly broad 2D band at 2720 cm^{-1} [40]. For GO (Figure 1j), both D and G bands became prominent and shifted at 1329 cm^{-1} and 1585 $cm^{-1,}$ representing the generation of sp^3 and sp^2 hybridized carbon atoms in graphene, respectively [41]. Compared with the GO spectrum, GOQDs-6 (Figure 1k) display that D and G bands are broader at 1337 cm^{-1} and 1593 cm^{-1}. In contrast, the peaks D and G are exhibited at 1341 cm^{-1} and 1581 cm^{-1} for GOQDs-8, see Figure 1l.

On the other hand, the identification of functional groups for GOQDs by Raman spectroscopy is complicated, and a deconvolution analysis is required [42,43]. Rajender G. and Giri P.K. reported a methodology for determining the D1, D2, and D3 bands in the region of the Raman spectrum from 1000 cm^{-1} to 1815 cm^{-1} by deconvolution utilizing Gaussian peaks [42]. They assigned D1 (~1185 cm^{-1}), D2 (~1260 cm^{-1}), and D3 (~1438 cm^{-1}) to the sp^2–sp^3 bonded carbon atoms at the edges of the GOQDs, COOH or ring type C–OH edge, and the C==O/C–O functional groups, respectively [42]. In our study, D1, D2, and D3 were determined utilizing this methodology, see Figures S1 and S2. For GOQDs-6 (Figure S1), the deconvoluted bands appear at 1104 cm^{-1} (D1), 1263 cm^{-1} (D2), and 1517 cm^{-1} (D3), while GOQDs-8 (Figure S2) bands are observed at 1116 cm^{-1} (D1), 1205 cm^{-1} (D2), and 1496 cm^{-1} (D3). The results by FTIR are consistent with these results.

The D-band and G-band intensities for GO, GOQDs-6, and GOQDs-8 were also utilized to calculate the I_D/I_G ratio. Compared to GO, the I_D/I_G value of GOQDs-6 increased from 1.04 to 1.08, suggesting that GOQDs possess some disordered structure than GO due to the presence of oxygen-rich molecules attached to the outside of aromatic C–C ring regions [43]. In contrast, the I_D/I_G value of GOQDs-8 decreased from 1.04 to 1.02, indicating that the amount of sp^3 hybridized carbon atoms in the graphitic network was enhanced. This finding suggests the obtention of high-quality GQDs [44]. Likewise, Ahirwar et al. reported an I_D/I_G superior to 1 for their GQDs/GOQDs, which was attributed to the presence of sp^3 carbon and functional groups on the surface [35].

Moreover, the crystallite size (L_a) can be estimated using the I_D/I_G ratio with Raman spectroscopy. The first empirical model for correlating L_a and I_D/I_G ratio was established by Tuinstra F. and Koenig J.L. [45]. Other models have been proposed to understand the relationship between L_a and I_D/I_G ratio [46,47]. Nevertheless, several approaches exist to elucidate this ratio, including the area (D-band and G-band) and deconvolution with the Lorentzian function, so they are the main drawback [48]. The I_D/I_G also changes significantly with the excitation energy, and the models are usually valid until 2 nm. Our

study obtained a L_a close to 10 nm under the Tuinstra and Koenig model. In contrast, a L_a close to 24 nm is observed according to the Cançado model [46]. This finding differs from the result obtained by XRD spectroscopy, which suggests that a Raman analysis with higher energy is necessary.

3.2. Morphological Characterization of GOQDs

TEM revealed that GOQDs-6 and GOQDs-8 exhibited nanoscale sizes around 2.5 nm and 2 nm, respectively, as a result of differences in synthesis conditions (Figure S3). Therefore, these findings provide support for XRD spectroscopy rather than Raman spectroscopy. Previously, an increment of electrochemical performance has been linked to smaller GQDs sizes mainly due to enhanced edge effect [23]. In order to differentiate the morphological structure of GOQDs materials exposed to different concentrations of HNO_3, micrographs of GOQDs-6 and GOQDs-8 are illustrated in Figure 2. HRTEM micrograph of GOQDs-6 (Figure 2a) illustrates the formation of GOQDs distributed over the graphene layer. Similar morphologies were observed by Dong et al. [21]. Moreover, HRTEM micrographs of GOQDs-6 clearly display the lattice structure of GOQDs. The lattice spacing was 0.2241 nm, corresponding to the crystalline plane 002, which represents the crystalline nature of GOQDs over the graphene layers, indicating the presence of sp^2 C–C bonding network for GQDs. Regarding the HRTEM micrograph of GOQDs-8 (Figure 2b), the image illustrates that the GOQDs have a quasi-spherical shape. Similar morphologies of GOQDs obtained with 8M of HNO_3 were reported by Shao et al. [19]. Compared with GOQDs-6, the lattice spacing was 0.2389 nm. The increment of the interplanar spacing in GOQDs-8 shows that the surface functionalization of GO suffered an increment in the number of anionic groups ($–COO^–$) that would potentially interact electrochemically with DA [26].

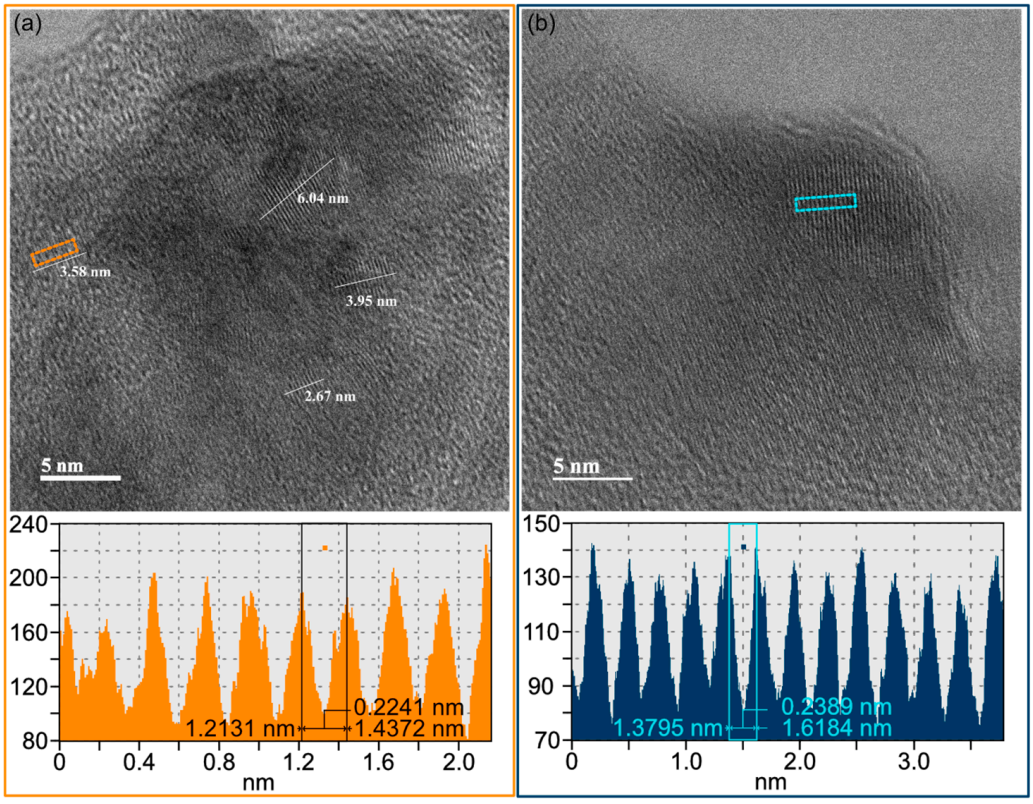


Figure 2. HRTEM of GOQDs, (**a**) GOQDs-6 and its lattice spacing measurement (orange); (**b**) GOQDs-8 and its lattice spacing measurement (blue).

The elemental content of the synthesized GOQDs materials was studied utilizing the Energy Dispersive Spectroscopy mapping technique (EDS). The EDS spectra of GOQDs-6 and GOQDs-8 are shown in Figure 3. Figure S4 displays pristine EDS. The spectrum confirms the presence of carbon and oxygen for both samples. Furthermore, the enhancement of HNO_3 concentration from 6 to 8 M resulted in an increase of the surface atomic percentage from 16.1% (in GOQDs-6) to 20.0% (in GOQDs-8), suggesting the addition of oxygen groups with a negative charge that would allow molecular interaction with DA.

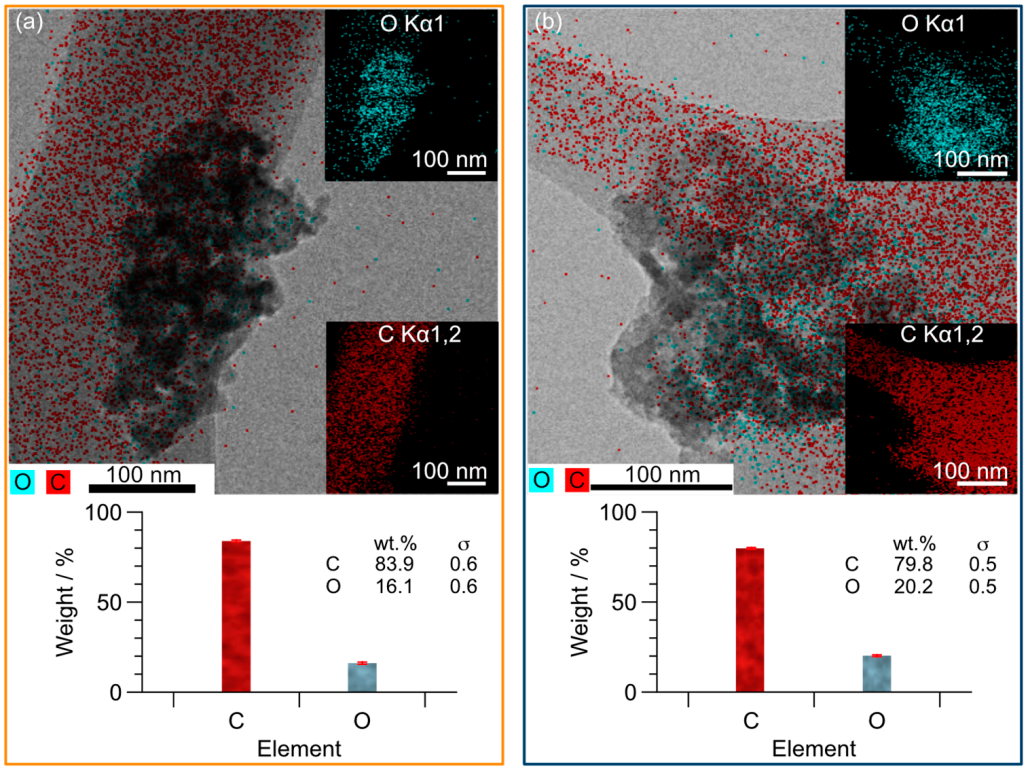


Figure 3. Energy Dispersive Spectroscopy mapping technique of GOQDs. (**a**) GOQDs-6; (**b**) GOQDs-8.

3.3. Cyclic Voltammetry Exploratory Study of DA

The structural and morphological characterization results support the functionalization and size dependence on synthesis conditions of GOQDs. The impact on surface modification of size and functionalization is expected to significantly influence DA detection, considering the inner-sphere mechanism of the molecule. To evaluate the GOQDs-6/GCE and GOQDs-8/GCE sensitivity towards DA, an explorative study was conducted comparing two configurations: GOQDs-6/GCE and GOQDs-8/GCE using CV at 50 mV/s with DA (50 µM). Figure 4a shows the voltammograms of both modified electrodes with an anodic peak around 0.18 V. The measured current at the electrode surface modified with GOQDs-6 was 1.3 µA while GQDs-8/GCE registered 2 µA for the same conditions, resulting in almost 2-fold improvement compared to bare GCE (1.1 µA). When analyzed at scan rates from 5 to 100 mV/s, the current grows proportionally to the square root of the scan rate, following a diffusion-controlled process for both materials (Figure 4b–e).

Moreover, the electrochemical oxidation-reduction mechanism of DA to dopamine orthoquinone (DAQ) has been demonstrated as an inner-sphere redox reaction; thus, there is a significant interaction between the DA and the GOQDs modified surface, which is crucial for electron transfer [49]. The inner sphere electron transfer process often involves electron transfer in an activated complex where a ligand is shared by an electronic conductor and the electroactive species [50]. In PBS (pH = 7.4) electrolyte, the positively charged DA can be attracted to the surface of negatively charged GQDs due to oxygen-rich groups

remaining after synthesis [51]. The π–π stacking or electrostatic attraction also allows increased DA sensing near the electrode surface, improving electron transfer and the registered current [52].

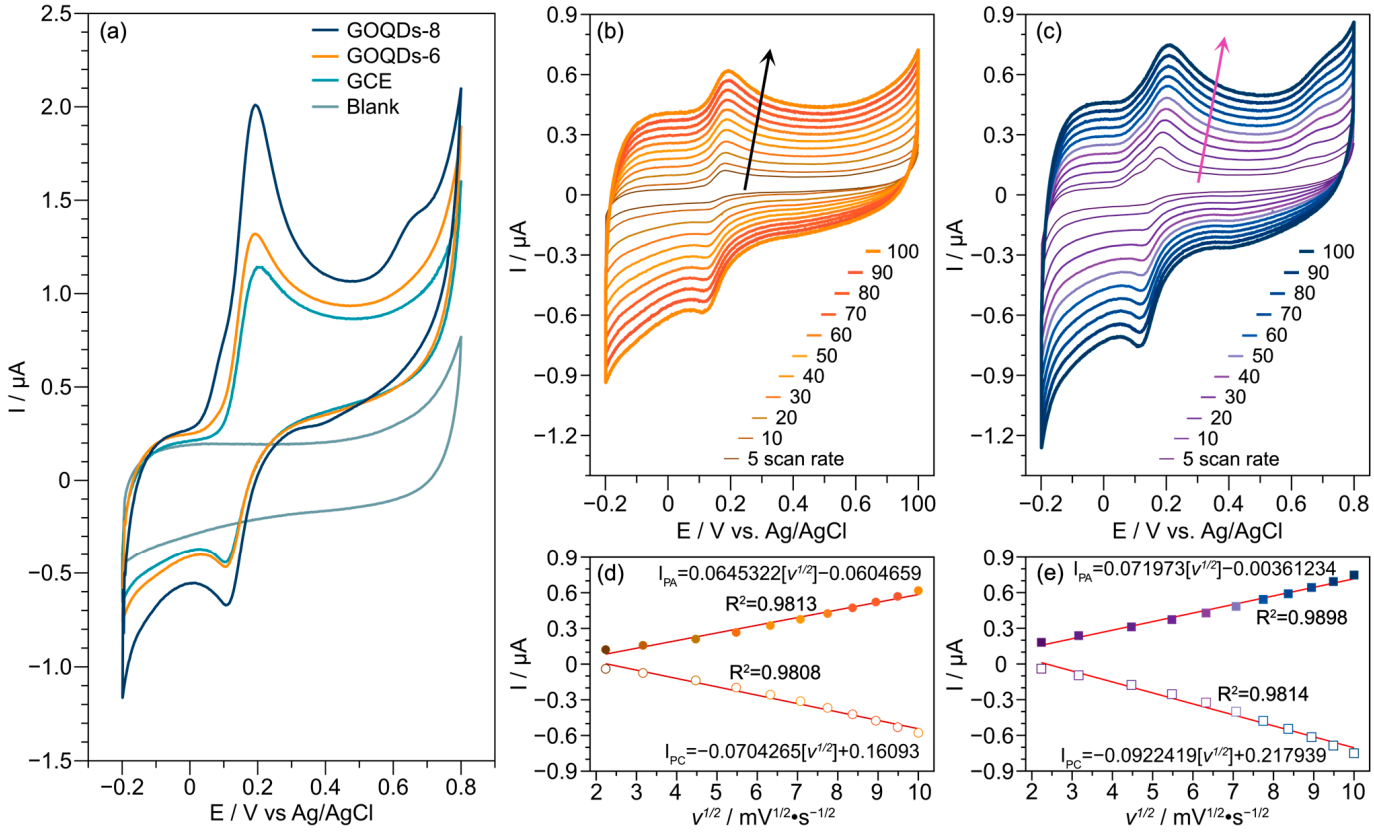


Figure 4. (**a**) CV of GOQDs-6, GOQDs-8, GCE, and blank analyzed with DA (50 µM); (**b**,**c**) CV of DA (10 µM) a different scan rate from 5 to 100 mV/s (black or purple arrow) for GOQDs-6 and GOQDs-8, respectively; (**d**,**e**) Plot of peak current anodic (I_a) and cathodic (I_c) vs. scan rate square root ($\nu^{1/2}$) for GOQDs-6 and GOQDs-8, respectively.

Figure 5 illustrates the proposed sensing mechanism between GOQDs and DA. Hawley M.D. and coworkers [5] studied the oxidation of catecholamines by an electrochemical technique, establishing that a quinone, in particular (DAQ), $2H^+$, and $2e^-$ were generated during the oxidation process. Furthermore, they found a slow cyclization rate for DA. Likewise, Sánchez-Rivera et al. [53] and, in another research by Shindler, S. and Bechtold, T. [54] reported DA pKa, which are $pKa_1 = 9.05$, $pKa_2 = 10.58$, and $pKa_3 = 12.07$ for –OH (C2), $-^+NH_3$, and –OH (C1), respectively, Figure 4b. Similarly, they reported a graph of the species distribution of DA in aqueous solution as a function of pH according to their pKA. At pH 7.4 (PBS buffer), most DA species are in their protonated amine form, although this region commences the dissociation of alcohol (C2). Overall, electrostatic attraction and the contribution of surface functionalization enhance DA detection at the GOQDs-modified electrode surface. Although both synthesized GOQDs can rely on this principle, the maximum response was obtained with GOQDs-8/GCE electrode due to higher GOQDs functionalization as described previously by XRD, FTIR, and EDS.

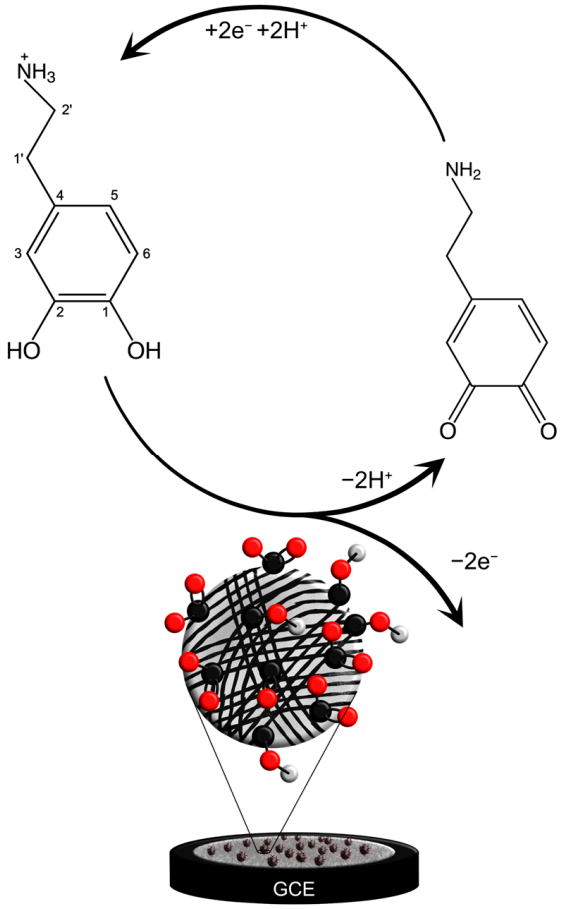


Figure 5. Proposed schematic mechanism for DA detection. Schematic diagram of GOQDs-6 or GOQDs-8 (red atoms are oxygen, black atoms are carbon) on the GCE are illustrated, which interacts with dopamine (DA) generating dopamine orthoquinone (DAQ), $2H^+$, and $2e^—$ during the oxidation process. Conversely, $2H^+$, and $2e^—$ are required to obtain DA.

3.4. Analytical Capabilities of GOQDs/GCE Sensor for DA Detection with Amperometry and DPV

DA oxidation in GOQDs-6/GCE and GOQDs-8/GCE can be exploited for analytical detection using amperometry (AMP), which involves measuring the current due to analyte oxidation at the modified electrode surface at a fixed potential. Furthermore, DA detection can be enhanced by increased surface area, edge effect of GOQDs, and DA absorption on electrode surface due to π-π interactions with sp^2 carbon in graphene-based materials and hydrogen bonding with oxygen-functional groups in GO [55]. Figure 6 shows a comparative of amperometric curves (i vs. t) of GOQDs-6/GCE and GOQDs-8/GCE sensors at fixed 0.18 V in two different concentration ranges: 0.1 to 1 μM, and 10 to 100 μM. The GOQDs/GCE sensors were subjected to different DA concentrations sequentially injected after 60 s; then, the increasing DA concentration resulted in a proportional anodic current registered for both modified electrodes. Notably, in all cases, the slope of GOQDs-8/GCE resulted superior to that of the GOQDs-6/GCE electrode, which is crucial, particularly at lower concentrations. For example, GOQDs-8/GCE has a sensitivity of 26.1 nAμM^{-1} and a LOD of 75.1 nM, while GOQDs-6/GCE has a sensitivity of 7.7 nA μM^{-1} and a LOD of 83.6 nM. In fact, in the 0.1 to 1 μM detection range, GOQDs-8/GCE slope was 3.5 fold higher than GOQDs-6/GCE, exhibiting 0.29 μA by each DA injection and a fast response time of 60 s. The sensitivity for GOQDs-8/GCE and GOQDs-6/GCE is 42.2 nA μM^{-1} and 12.0 nA μM^{-1}, respectively, while the LOD is 17.6 nM and 70.6 nM.

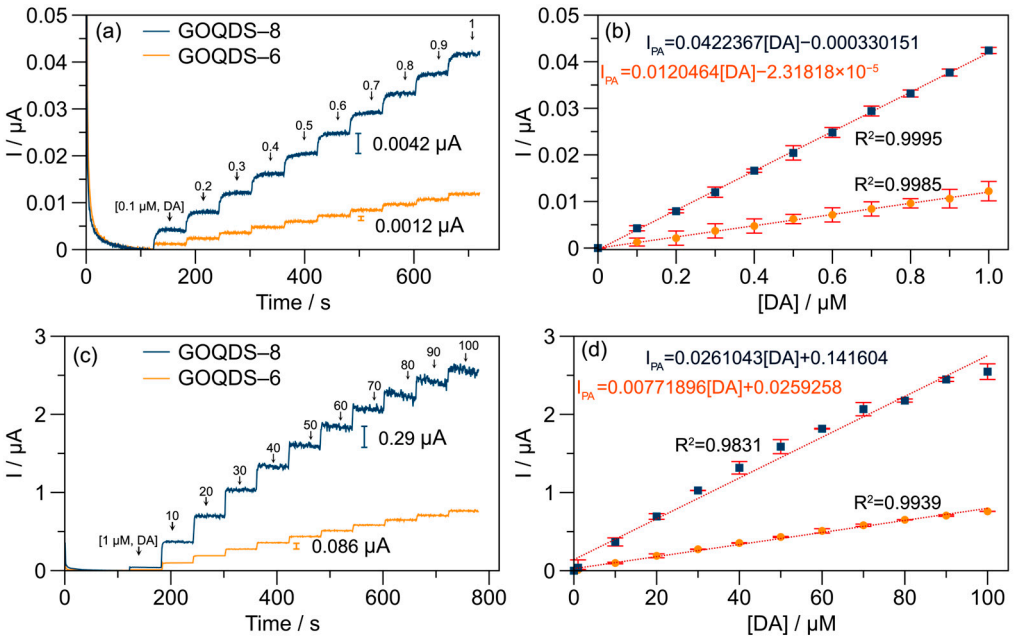


Figure 6. Amperometry curves for GOQDS-6/GCE and GOQDS-8/GCE. (**a**) Amperometric curves from 0.1 μM to 1 μM; (**b**) Calibration curve from 0.1 μM to 1 μM. (**c**) Amperometric curves from 1 μM to 100 μM; (**d**) Calibration curve from 1 μM to 100 μM.

Dai et al. [56] reported the amperometric curves for AuPd@Fe_2O_3 Nps/GCE with successive injection of DA from 0.01 μM to 832 μM in PBS (pH 5.5) at a potential applied of 0.48 V. They also found the LOD with a value of 0.01 μM and a sensitivity of 4.89 nAμM^{-1}. In fact, the sensitivity is 8-fold in the range from 0.1 μM to 1 μM DA in our study.

The synthesis of materials with high functional group content and its incorporation into the working electrode, particularly carboxylic acid, is vital to increase DA sensing due to the enhancement in the active sites and therefore, allow a faster electron transfer. The COO^- groups enhance the sensitivity and selectivity of DA due to the formation of intermolecular forces between them and DA [57]. When comparing GOQDs-8/GCE and GOQDs-6/GCE, the GCE electrode exhibits a diminished amperometry response with an average enhancement of 0.029 μA, see Figure S5. Thus, the functionalization of materials is crucial for DA sensing, confirmed by this finding.

Differential pulse voltammetry (DPV) is a sensitive electroanalytical technique that has been demonstrated to be sensitive to DA detection and useful for analysis in complex matrices. Considering the performance shown in AMP, only the GOQDs-8/GCE sensor was evaluated with DPV for DA detection. Figure 7a displays a characteristic anodic current with a maximum potential of 0.16 V, which increases along with DA concentration, suggesting that the GOQDs-8/GCE sensor is sensitive towards DA [26].

Additionally, Figure 7b illustrates the calibration curves obtained from GOQDs-8/GCE electrodes where the current response was plotted as a function of DA concentration. A polynomial equation was found in the concentration range of 1 to 100 μM DA. Nonetheless, the GOQDs-8/GCE sensor exhibited a DA saturation on the electrode surface > 30 μM. The relationship between DA concentration and the peak current at 0.16 V was represented by the regression equation $I_{PA} = 4.589 \times 10^{-6}$ $[DA]^3 - 1.071 \times 10^{-3}$ $[DA]^2 + 0.0883$ $[DA] - 0.029$ ($R^2 = 0.9995$, n = 11). The estimated LOD and sensitivity for this assay were 506 nM and 0.061 μAμM^{-1}, respectively. These values were calculated utilizing the linear function ($I_{PA} = 0.0616742$ [DA] + 0.0316569) below 30 μM of DA. To verify this LOD value, a study of DA concentration in this region was conducted, see Figure S6. The performance can be correlated with the sensing mechanism, where the higher functionalization of the

GOQDs-8 surfaces indicates an analytical improvement. This opinion is supported by the GCE analysis in PBS using DPV, see Figure S7, where GQDs-8 has 3-fold the current of GCE at 30 µM.

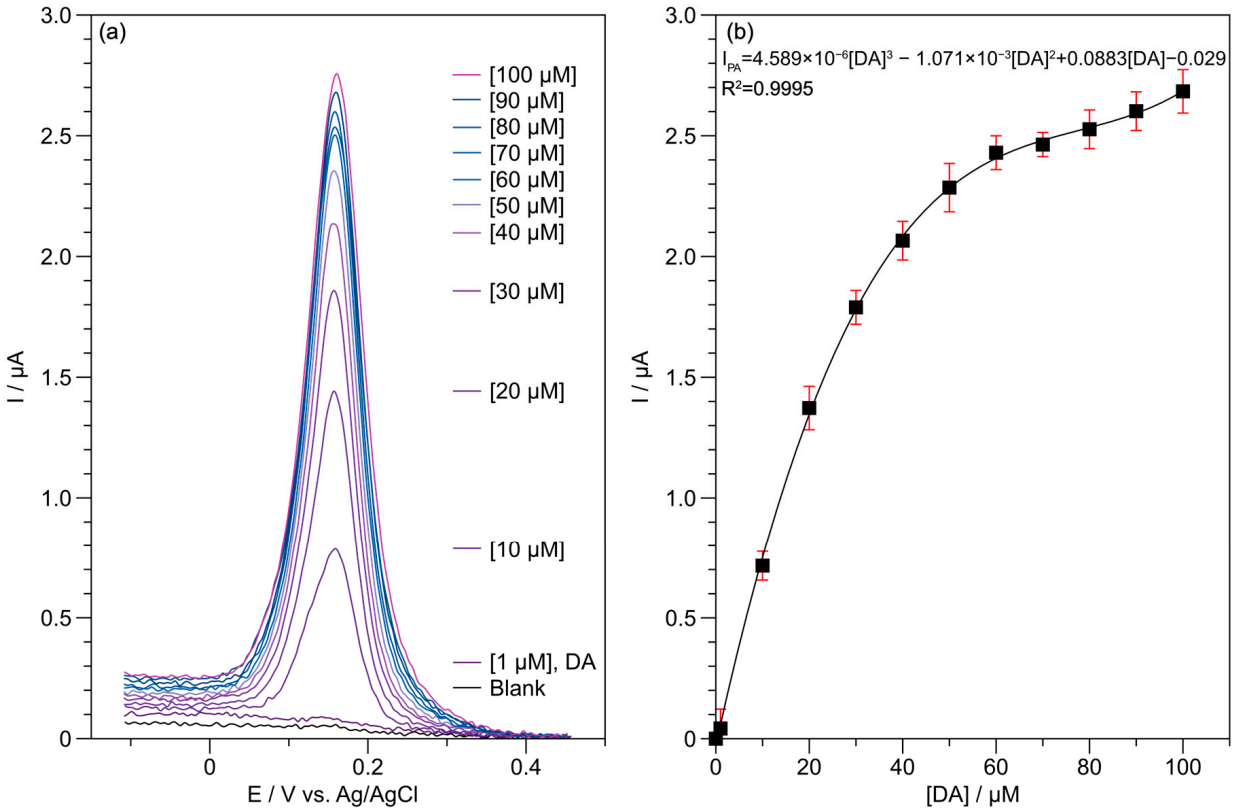


Figure 7. (**a**) DPV for GOQDS-8/GCE in PBS (pH = 7.4); (**b**) Calibration curves obtained by DPV for GOQDS-8/GCE in PBS (pH = 7.4).

In our study, the polynomial regression is contrary to Zheng et al. [26], who reported a linear behavior for their sensor GQDs/GCE with a linear range from 0.4 to 100 µM, a LOD of 0.05 µM and a correlation coefficient of 0.997 by DPV.

In contrast, Balkourani et al. [58] reported two linear increase trends regarding DA concentration for Ti_{NCs}/G_m-Cu_{foil} sensor, the first from 10 µM to 90 µM and the second linear range from 100 µM to 400 µM DA with a correlation coefficient of 0.995 and 0.987, respectively. Similarly, Xu et al. [59] reported the intercalation transition of metal oxide into graphite powder, observing two linear regions with increased DA concentration.

Figure 8 displays a comparative of the selectivity of GQDs-8/GCE when evaluated using either AMP (Figure 8a) or DPV (Figure 8b) against interference, including uric acid (UA), ascorbic acid (AA), acetaminophen (AC), and L-DOPA. Although AMP resulted in lower LOD, the potential oxidation of AA close to DA potential resulted in interference from both compounds. However, this could be mainly solved with a Nafion layer to depley AA molecules at the electrode surface; the same GOQDs-8/GCE sensor electrode showed a satisfactory selectivity towards AA, DA, and UA when evaluated using DPV [60]. This selectivity is characteristic of DPV, where the technique is effective for canceling background current and improving signal-to-noise ratio, which allows a selective detection of the target analyte. However, both techniques demonstrated the enhanced analytical capabilities of the system due to the addition of functionalized GOQDs. Figure S8 displays DPV curves of DA, L-DOPA, UA, and AC (10 µM) on GQDs-8/GCE in PBS at a pH of 7.4.

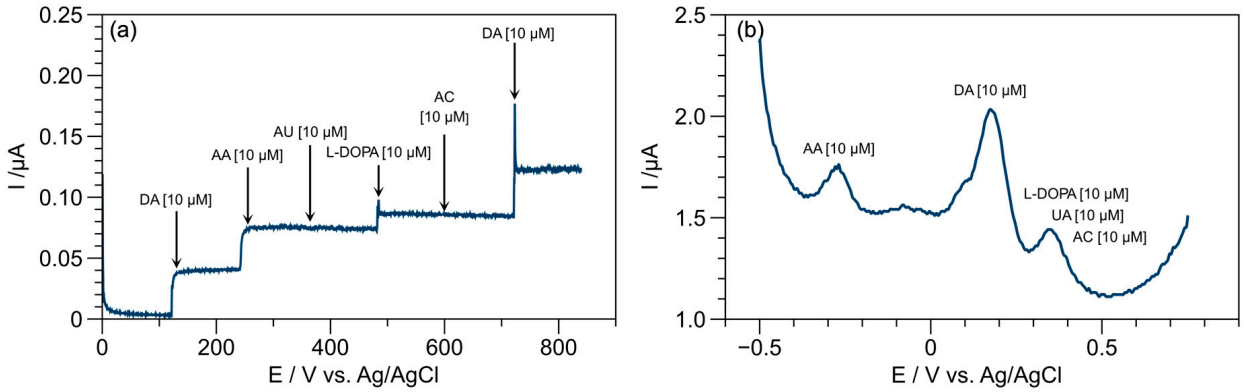


Figure 8. Selectivity of GQDS-8/GCE against DA, ascorbic acid (AA), uric acid (UA), levodopa (L-DOPA), and acetaminophen (AC) interferences. (**a**) AMP; (**b**) DPV.

3.5. Detection of DA in Normal Human Serum

Figure 9a displays the evaluation of the feasibility of GOQDS-8/GCE for the detection of DA in normal human serum (NHS) by DPV. The concentration of DA exhibits an increase in DPV curves, which is similar to the response of DPV in PBS (Figure 7a). Figure 7b illustrates the calibration curve in NHS with PBS at a pH of 7.4 and DA concentration from 0.55 to 50 µM. The curve regression is a polynomial with a coefficient correlation of 0.9992 (n = 10).

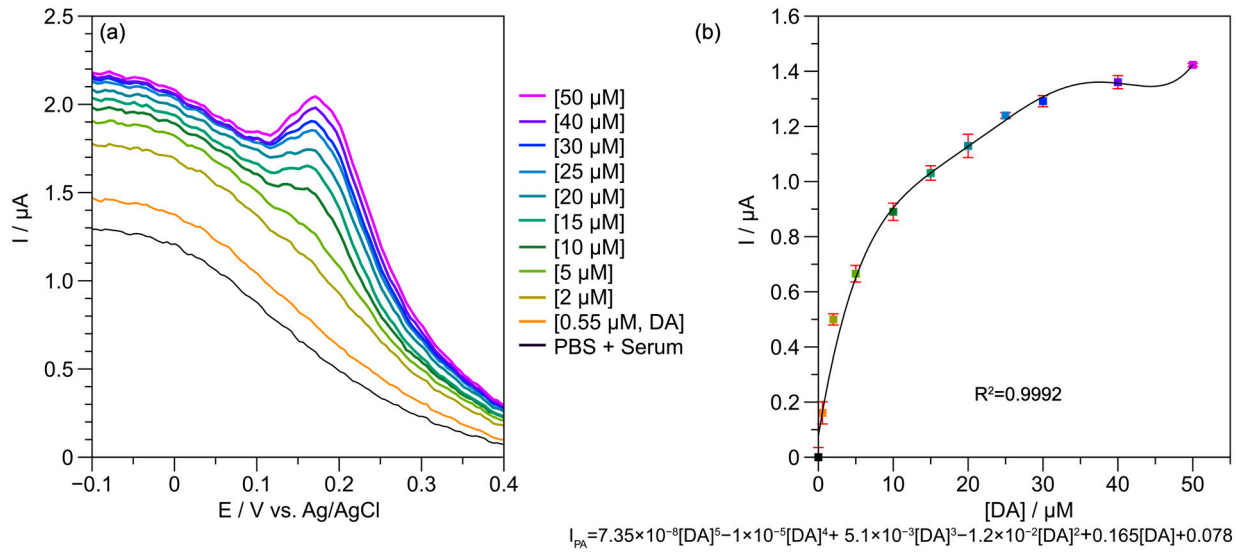


Figure 9. (**a**) DPV for GOQDS-8/GCE in PBS and normal human serum (pH = 7.4); (**b**) Calibration curves obtained by DPV for GOQDS-8/GCE in PBS and normal human serum (NHS) (pH = 7.4).

Table 1 illustrates DA detection in NHS using the GOQDs-8/GCE sensor. The sensor shows adequate performance at evaluated DA concentrations. The recovery was in the range of 94.1 to 112.8% with a relative standard deviation (RSD), n = 3 of less than 3.62%. These results are consistent with other systems utilizing fetal bovine serum and human serum reported in the scientific literature for DA detection. For example, Carvalho da Silva et al. reported a sensor PGE/NiTsPc-ZnONPs-CNT to detect DA by CV with a recovery of approximately 102% [61]. Likewise, Gong evaluated the feasibility of the sensor P-L-Trp/GN/GCE for DA determination by DPV and found recovery rates between 100.4% and 104.4% [62].

Table 1. DA detection in NHS for GQDs-8/GCE.

Added (DA, μM)	Found (DA, μM)	Recovery (%)	RSD * (%) (n = 3)
0	-	-	6.41
3.5	3.95	112.8	2.89
7.5	7.05	94.1	3.62
12.5	12.29	98.3	1.31
17.5	19.04	108.8	0.92
22.5	22.95	102.0	0.85

* RSD = relative standard deviation.

Table 2 illustrates a comparison of electrochemical sensors for DA detection modified with either GQDs or GOQDs from different precursors such as citric acid, glucose, polymers, or GO. Although they showed superior analytical performance, the current approach focused on the effect of synthesis conditions on the final electrochemical detection of DA. The synergistic effects of electrostatic attraction, functionalization for inner-sphere mechanism, and edge effect from smaller particle sizes resulted in amplified electrochemical signal achieving detection at the nanomolar level using AMP and DPV. Moreover, the GCE/GOQDs-8 showed minimal response towards easily oxidized interferences such as UA, AA, AC, and L-DOPA. Comparatively, the GOQDs-8/GCE sensor showed an effective use of the modified nanocarbon layer, achieving relevant analytical figures with a simpler composite. Moreover, since the contribution of GOQDs-8 for sensing was established, the system can be further improved by combining with polymeric supports, metallic nanoparticles, or additional carbon nanomaterials.

Table 2. GQDs and GOQDs sensors for electrochemical detection of DA.

Sensor	Precursor	Technique	Linear Range (μM)	Sensitivity (μA μM^{-1})	LOD	Ref
GQDs/GCE	Citric acid	DPV	0.4–100	1.0–200	50 nM	[26]
GQDs–ethylenediamine/GCE	Citric acid	DPV	1–150	-	0.115 μM	[25]
GQDs@MWCNTs/GCE	Glucose	DPV	0.25–250	-	0.095 μM	[63]
GOQDS-Nafion/GCE	GO	DPV	0.005–100	0.0859	0.00045 μM	[64]
GOQDs-MWCNTs/GCE	GO	DPV	0.005–100	-	0.87 nM	[65]
N-GQDs/GCE	Polyndole	DPV	0.001–1000	10.25 and 15.95	0.15 nM	[28]
GQDs/GCE	Polyacrylonitrile	DPV	3–100	-	-	[27]
GQD/SPE	Citric acid	DPV	0.1–1000	0.0745	0.05 μM	[66]
CS/N,GQDs@SPE	Glucose	DPV	1.0–200	418 *	0.145 μM	[67]
GOQDs-8/GCE	GO	AMP	0.1–1	0.0422	17.6 nM	
GOQDs-6/GCE	GO	AMP	0.1–1	0.0120	70.6 nM	This
GOQDs-8/GCE	GO	AMP	1–100	0.0261	75.1 nM	work
GOQDs-6/GCE	GO	AMP	1–100	0.0077	83.6 nM	
GOQDs-8/GCE	GO	DPV	0.1–30	0.0616	506 nM	

* μA Mm^{-1} cm^{-2}.

4. Conclusions

In this work, we presented a sensitive and selective electrochemical GOQDs/GCE sensor for the detection of DA. The liquid-phase oxidation reaction of GO with HNO_3 (6 and 8 M) allowed to obtain two GOQDs (GOQDs-6 and GOQDs-8) with differences in the content of functional groups due to synthesis and their characterization by XRD, HR-TEM, FTIR, and RAMAN. GCE functionalization with GOQDs-8 showed an enhanced electrochemical response towards DA ascribed to their smaller size and high functionalization that facilitate the inner-sphere DA redox reaction mechanism. The evaluation of GOQDs-8/GCE showed a more sensitive behavior by the amperometry technique; however, it was more

selective by differential pulse voltammetry. Compared to GOQDs-8/GCE, GOQDs-6/GCE had a lower performance. The presented approach with a three-electrode system detection allowed a real-time detection of DA, representing a promising alternative for the diagnosis of neurodevelopmental disorders being able to detect low concentrations of DA. In addition, through the normal human serum assay, the sensor GOQDs-8/GCE proved to be relatively well feasible for the practical determination of DA.

Supplementary Materials: The following supporting information can be downloaded at: https://www.mdpi.com/article/10.3390/chemosensors13010007/s1, Figure S1. Deconvolution of D1, D2, D3 peaks for GOQDs-6. Figure S2. Deconvolution of D1, D2, D3 peaks for GOQDs-8. Figure S3. TEM images of (a) GOQDs-6 and (b) GOQDs-8. Figure S4. Energy Dispersive Spectroscopy mapping technique of GOQDs. (a) GOQDs-6; (b) GOQDs-8. Figure S5. Amperometry curves for GOQDS-8/GCE, GOQDS-6/GCE and GCE from 1 μM to 90 μM of DA. Figure S6. DPV curves for GOQDS-8/GCE from 0.3 to 0.8 μM DA. Figure S7. DPV curves for GCE from 5 to 30 μM DA. Figure S8. Selectivity of GQDS-8/GCE against uric acid (UA), acetaminophen (AC), and Levodopa (L-DOPA) interferences and its comparison with dopamine (DA) by DPV.

Author Contributions: Conceptualization, V.O. and O.I.T.-S.; methodology, investigation, formal analysis O.I.T.-S.; investigation, formal analysis, R.B.D., V.O. and A.V.-R.; data curation, A.V.-R.; writing—original draft preparation, O.I.T.-S., A.V.-R., R.B.D. and V.O.; writing—review and editing O.I.T.-S., A.V.-R., R.B.D. and V.O.; supervision, V.O.; funding acquisition, R.B.D. and A.V.-R. All authors have read and agreed to the published version of the manuscript.

Funding: This research was funded by Centro de Investigación en Materiales Avanzados, S.C., grant number 26018.

Institutional Review Board Statement: Not applicable.

Informed Consent Statement: Not applicable.

Data Availability Statement: The original contributions presented in this study are included in the article/Supplementary Materials. Further inquiries can be directed to the corresponding author.

Acknowledgments: The authors would like to thank CONHACYT for the scholarship granted to Omar Isaac Torres Soto (826785). We also would like to thank Andres Isaak Gonzalez Jacquez, Luis de la Torre Saenz, Pedro Piza Ruiz, Raul Armando Ochoa Gamboa, and Marco Antonio Ruiz Esparza for their technical assistance.

Conflicts of Interest: The authors declare no conflicts of interest.

References

1. Duszkiewicz, A.J.; McNamara, C.G.; Takeuchi, T.; Genzel, L. Novelty and Dopaminergic Modulation of Memory Persistence: A Tale of Two Systems. *Trends Neurosci.* **2019**, *42*, 102–114. [CrossRef]
2. Pan, X.; Kaminga, A.C.; Wen, S.W.; Wu, X.; Acheampong, K.; Liu, A. Dopamine and Dopamine Receptors in Alzheimer's Disease: A Systematic Review and Network Meta-Analysis. *Front. Aging Neurosci.* **2019**, *11*, 175. [CrossRef] [PubMed]
3. Chauhan, N.; Soni, S.; Agrawal, P.; Balhara, Y.P.S.; Jain, U. Recent advancement in nanosensors for neurotransmitters detection: Present and future perspective. *Process. Biochem.* **2020**, *91*, 241–259. [CrossRef]
4. Mandic-Maravic, V.; Grujicic, R.; Milutinovic, L.; Munjiza-Jovanovic, A.; Pejovic-Milovancevic, M. Dopamine in Autism Spectrum Disorders—Focus on D2/D3 Partial Agonists and Their Possible Use in Treatment. *Front. Psychiatry* **2022**, *12*, 787097. [CrossRef]
5. Hawley, M.D.; Tatawawadi, S.V.; Piekarski, S.; Adams, R.N. Electrochemical Studies of the Oxidation Pathways of Catecholamines. *J. Am. Chem. Soc.* **1967**, *89*, 447–450. [CrossRef]
6. Harrison, W.H.; Whisler, W.W.; Hill, B.J. Catechol amine oxidation and ionization properties indicated from the hydrogen ion release, tritium exchange, and spectral changes which occur during ferricyanide oxidation. *Biochemistry* **1968**, *7*, 3089–3094. [CrossRef] [PubMed]
7. Karim, A.; Yasser, M.; Ahmad, A.; Natsir, H.; Wahab, A.W.; Fauziah, S.; Taba, P.; Pratama, I.; Rosalin; Rajab, A.; et al. A review: Progress and trend advantage of dopamine electrochemical sensor. *J. Electroanal. Chem.* **2024**, *959*, 118157. [CrossRef]

8. Balkourani, G.; Brouzgou, A.; Tsiakaras, P. A review on recent advancements in electrochemical detection of dopamine using carbonaceous nanomaterials. *Carbon* **2023**, *213*, 118281. [CrossRef]
9. Sternson, A.W.; McCreery, R.; Feinberg, B.; Adams, R.N. Electrochemical Studies of Adrenergic Neurotransmitters and Related Compounds. *J. Electroanal. Chem. Interfacial Electrochem.* **1973**, *46*, 313–321. [CrossRef]
10. Tse, D.C.S.; McCreery, R.L.; Adams, R.N. Potential oxidative pathways of brain catecholamines. *J. Med. Chem.* **1976**, *19*, 37–40. [CrossRef] [PubMed]
11. Dayton, M.A.; Ewing, A.G.; Wightman, R.M. Response of microvoltammetric electrodes to homogeneous catalytic and slow heterogeneous charge-transfer reactions. *Anal. Chem.* **1980**, *52*, 2392–2396. [CrossRef]
12. Dayton, M.A.; Brown, J.C.; Stutts, K.J.; Wightman, R.M. Faradaic electrochemistry at microvoltammetric electrodes. *Anal. Chem.* **1980**, *52*, 946–950. [CrossRef]
13. Anjo, D.M.; Kahr, M.; Khodabakhsh, M.M.; Nowinski, S.; Wanger, M. Electrochemical activation of carbon electrodes in base: Minimization of dopamine adsorption and electrode capacitance. *Anal. Chem.* **1989**, *61*, 2603–2608. [CrossRef]
14. Wester, N.; Sainio, S.; Palomäki, T.; Nordlund, D.; Singh, V.K.; Johansson, L.-S.; Koskinen, J.; Laurila, T. Partially Reduced Graphene Oxide Modified Tetrahedral Amorphous Carbon Thin-Film Electrodes as a Platform for Nanomolar Detection of Dopamine. *J. Phys. Chem. C* **2017**, *121*, 8153–8164. [CrossRef]
15. Sharel, P.E.; Miller, T.S.; Macpherson, J.V.; Unwin, P.R. Controlled functionalisation of single-walled carbon nanotube network electrodes for the enhanced voltammetric detection of dopamine. *Phys. Chem. Chem. Phys.* **2015**, *17*, 26394–26402. [CrossRef]
16. Tshangana, C.S.; Muleja, A.A.; Kuvarega, A.T.; Malefetse, T.J.; Mamba, B.B. The applications of graphene oxide quantum dots in the removal of emerging pollutants in water: An overview. *J. Water Process. Eng.* **2021**, *43*, 102249. [CrossRef]
17. Yan, X.; Cui, X.; Li, L. Synthesis of Large, Stable Colloidal Graphene Quantum Dots with Tunable Size. *J. Am. Chem. Soc.* **2010**, *132*, 5944–5945. [CrossRef]
18. Dong, Y.; Lin, J.; Chen, Y.; Fu, F.; Chi, Y.; Chen, G. Graphene quantum dots, graphene oxide, carbon quantum dots and graphite nanocrystals in coals. *Nanoscale* **2014**, *6*, 7410–7415. [CrossRef]
19. Shao, T.; Wang, G.; An, X.; Zhuo, S.; Xia, Y.; Zhu, C. A reformative oxidation strategy using high concentration nitric acid for enhancing the emission performance of graphene quantum dots. *RSC Adv.* **2014**, *4*, 47977–47981. [CrossRef]
20. Zhao, M. Direct Synthesis of Graphene Quantum Dots with Different Fluorescence Properties by Oxidation of Graphene Oxide Using Nitric Acid. *Appl. Sci.* **2018**, *8*, 1303. [CrossRef]
21. Dong, Y.; Zhang, S.; Shi, L.; Chen, Y.; Ma, J.; Guo, S.; Chen, X.; Song, H. The photoluminescence of step-wise reduced graphene oxide quantum dots. *Mater. Chem. Phys.* **2018**, *203*, 125–132. [CrossRef]
22. Buatong, N.; Ruttanapun, C.; Sriwong, C. Synthesis of reduced graphene oxide quantum dots from graphene oxide via hydrothermal process and theirs structural, luminescence and magnetic properties. *J. Taiwan Inst. Chem. Eng.* **2023**, *142*, 104667. [CrossRef]
23. Facure, M.H.M.; Schneider, R.; Lima, J.B.S.; Mercante, L.A.; Correa, D.S. Graphene Quantum Dots-Based Nanocomposites Applied in Electrochemical Sensors: A Recent Survey. *Electrochem* **2021**, *2*, 490–519. [CrossRef]
24. Kalkal, A.; Kadian, S.; Pradhan, R.; Manik, G.; Packirisamy, G. Recent advances in graphene quantum dot-based optical and electrochemical (bio)analytical sensors. *Mater. Adv.* **2021**, *2*, 5513–5541. [CrossRef]
25. Li, Y.; Jiang, Y.; Mo, T.; Zhou, H.; Li, Y.; Li, S. Highly selective dopamine sensor based on graphene quantum dots self-assembled monolayers modified electrode. *J. Electroanal. Chem.* **2016**, *767*, 84–90. [CrossRef]
26. Zheng, S.; Huang, R.; Ma, X.; Tang, J.; Li, Z.; Wang, X.; Wei, J.; Wang, J. A Highly Sensitive Dopamine Sensor Based on Graphene Quantum Dots Modified Glassy Carbon Electrode. *Int. J. Electrochem. Sci.* **2018**, *13*, 5723–5735. [CrossRef]
27. Chen, A.; Zhao, C.; Yu, Y.; Yang, J. Graphene quantum dots derived from carbon fibers for oxidation of dopamine. *J. Wuhan Univ. Technol. Mater. Sci. Ed.* **2016**, *31*, 1294–1297. [CrossRef]
28. Thadathil, A.; Thacharakkal, D.; Ismail, Y.A.; Periyat, P. Polyindole-Derived Nitrogen-Doped Graphene Quantum Dots-Based Electrochemical Sensor for Dopamine Detection. *Biosensors* **2022**, *12*, 1063. [CrossRef]
29. Hummers, W.S.; Offeman, R.E. Preparation of Graphitic Oxide. *J. Am. Chem. Soc.* **1958**, *80*, 1339. [CrossRef]
30. Elgrishi, N.; Rountree, K.J.; McCarthy, B.D.; Rountree, E.S.; Eisenhart, T.T.; Dempsey, J.L. A Practical Beginner's Guide to Cyclic Voltammetry. *J. Chem. Educ.* **2018**, *95*, 197–206. [CrossRef]
31. Popova, A.N. Crystallographic analysis of graphite by X-Ray diffraction. *Coke Chem.* **2017**, *60*, 361–365. [CrossRef]
32. Krishnamoorthy, K.; Veerapandian, M.; Yun, K.; Kim, S.-J. The chemical and structural analysis of graphene oxide with different degrees of oxidation. *Carbon* **2013**, *53*, 38–49. [CrossRef]
33. Huang, H.-H.; De Silva, K.K.H.; Kumara, G.R.A.; Yoshimura, M. Structural Evolution of Hydrothermally Derived Reduced Graphene Oxide. *Sci. Rep.* **2018**, *8*, 6849. [CrossRef] [PubMed]
34. Shooshtari, M. Ammonia gas sensors based on multi-wall carbon nanofiber field effect transistors by using gate modulation. *Colloids Surf. A Physicochem. Eng. Asp.* **2025**, *704*, 135563. [CrossRef]

35. Ahirwar, S.; Mallick, S.; Bahadur, D. Electrochemical Method To Prepare Graphene Quantum Dots and Graphene Oxide Quantum Dots. *ACS Omega* **2017**, *2*, 8343–8353. [CrossRef] [PubMed]
36. Kumar, S.; Ojha, A.K.; Ahmed, B.; Kumar, A.; Das, J.; Materny, A. Tunable (violet to green) emission by high-yield graphene quantum dots and exploiting its unique properties towards sun-light-driven photocatalysis and supercapacitor electrode materials. *Mater. Today Commun.* **2017**, *11*, 76–86. [CrossRef]
37. Chen, Z.; Xia, M.; Gao, Y.; Ma, W.; Chen, Y.; Wang, X.; Chen, H.; Yang, H. Study of the effect of nitric acid on the structure and optical properties of alkali lignin-based carbon dots. *Carbon Capture Sci. Technol.* **2024**, *12*, 100218. [CrossRef]
38. Zhang, Y.-P.; Ma, J.-M.; Yang, Y.-S.; Ru, J.-X.; Liu, X.-Y.; Ma, Y.; Guo, H.-C. Synthesis of nitrogen-doped graphene quantum dots (N-GQDs) from marigold for detection of Fe3+ ion and bioimaging. *Spectrochim. Acta A Mol. Biomol. Spectrosc.* **2019**, *217*, 60–67. [CrossRef]
39. Orlando, A.; Franceschini, F.; Muscas, C.; Pidkova, S.; Bartoli, M.; Rovere, M.; Tagliaferro, A. A Comprehensive Review on Raman Spectroscopy Applications. *Chemosensors* **2021**, *9*, 262. [CrossRef]
40. Ramya, A.V.; Manoj, B.; Mohan, A.N. Extraction and Characterization of Wrinkled Graphene Nanolayers from Commercial Graphite. *Asian J. Chem.* **2016**, *28*, 1031–1034. [CrossRef]
41. Stankovich, S.; Dikin, D.A.; Piner, R.D.; Kohlhaas, K.A.; Kleinhammes, A.; Jia, Y.; Wu, Y.; Nguyen, S.T.; Ruoff, R.S. Synthesis of graphene-based nanosheets via chemical reduction of exfoliated graphite oxide. *Carbon* **2007**, *45*, 1558–1565. [CrossRef]
42. Rajender, G.; Giri, P.K. Formation mechanism of graphene quantum dots and their edge state conversion probed by photoluminescence and Raman spectroscopy. *J. Mater. Chem. C* **2016**, *4*, 10852–10865. [CrossRef]
43. Ke, Z.; Azam, M.; Ali, S.; Zubair, M.; Cao, Y.; Khan, A.A.; Hassan, A.; Xue, W. Role of Functional Groups in Tuning Luminescence Signature of Solution-Processed Graphene Quantum Dots: Experimental and Theoretical Insights. *Molecules* **2024**, *29*, 2790. [CrossRef] [PubMed]
44. Dervishi, E.; Ji, Z.; Htoon, H.; Sykora, M.; Doorn, S.K. Raman spectroscopy of bottom-up synthesized graphene quantum dots: Size and structure dependence. *Nanoscale* **2019**, *11*, 16571–16581. [CrossRef]
45. Tuinstra, F.; Koenig, J.L. Raman Spectrum of Graphite. *J. Chem. Phys.* **1970**, *53*, 1126–1130. [CrossRef]
46. Cançado, L.G.; Jorio, A.; Ferreira, E.H.M.; Stavale, F.; Achete, C.A.; Capaz, R.B.; Moutinho, M.V.O.; Lombardo, A.; Kulmala, T.S.; Ferrari, A.C. Quantifying Defects in Graphene via Raman Spectroscopy at Different Excitation Energies. *Nano Lett.* **2011**, *11*, 3190–3196. [CrossRef] [PubMed]
47. Cançado, L.G.; Monken, V.P.; Campos, J.L.E.; Santos, J.C.C.; Backes, C.; Chacham, H.; Neves, B.R.A.; Jorio, A. Science and Metrology of defects in graphene using Raman Spectroscopy. *Carbon* **2024**, *220*, 118801. [CrossRef]
48. Zickler, G.A.; Smarsly, B.; Gierlinger, N.; Peterlik, H.; Paris, O. A reconsideration of the relationship between the crystallite size La of carbons determined by X-ray diffraction and Raman spectroscopy. *Carbon* **2006**, *44*, 3239–3246. [CrossRef]
49. Ghilane, J.; Hauquier, F.; Lacroix, J.-C. Oxidative and Stepwise Grafting of Dopamine Inner-Sphere Redox Couple onto Electrode Material: Electron Transfer Activation of Dopamine. *Anal. Chem.* **2013**, *85*, 11593–11601. [CrossRef] [PubMed]
50. Bard, A.J. Inner-Sphere Heterogeneous Electrode Reactions. Electrocatalysis and Photocatalysis: The Challenge. *J. Am. Chem. Soc.* **2010**, *132*, 7559–7567. [CrossRef]
51. Rahman, M.M.; Lee, J.-J. Electrochemical Dopamine Sensors Based on Graphene. *J. Electrochem. Sci. Technol.* **2019**, *10*, 185–195. [CrossRef]
52. Gao, F.; Cai, X.; Wang, X.; Gao, C.; Liu, S.; Gao, F.; Wang, Q. Highly sensitive and selective detection of dopamine in the presence of ascorbic acid at graphene oxide modified electrode. *Sens. Actuators B Chem.* **2013**, *186*, 380–387. [CrossRef]
53. Sánchez-Rivera, A.E.; Corona-Avendaño, S.; Alarcón-Angeles, G.; Rojas-Hernández, A.; Ramírez-Silva, M.T.; Romero-Romo, M.A. Spectrophotometric study on the stability of dopamine and the determination of its acidity constants. *Spectrochim. Acta A Mol. Biomol. Spectrosc.* **2003**, *59*, 3193–3203. [CrossRef]
54. Schindler, S.; Bechtold, T. Mechanistic insights into the electrochemical oxidation of dopamine by cyclic voltammetry. *J. Electroanal. Chem.* **2019**, *836*, 94–101. [CrossRef]
55. Wang, Y.; Li, Y.; Tang, L.; Lu, J.; Li, J. Application of graphene-modified electrode for selective detection of dopamine. *Electrochem. Commun.* **2009**, *11*, 889–892. [CrossRef]
56. Dai, M.; Zhu, Q.; Han, D.; Niu, L.; Wang, Z. Sensitive and selective electrochemical sensor for the detection of dopamine by using AuPd@Fe2O3 nanoparticles as catalyst. *Adv. Sens. Energy Mater.* **2023**, *2*, 100048. [CrossRef]
57. Burns, G.; Ali, M.Y.; Howlader, M.M.R. Advanced functional materials for electrochemical dopamine sensors. *TrAC Trends Anal. Chem.* **2023**, *169*, 117367. [CrossRef]
58. Balkourani, G.; García-Martín, J.M.; Gorbova, E.; Vecchio, C.L.; Baglio, V.; Brouzgou, A.; Tsiakaras, P. Electrochemical Detection of Dopamine: Novel Thin-Film Ti-Nanocolumnar Arrays/Graphene Monolayer-Cufoil Electrodes. *Catalysts* **2024**, *14*, 478. [CrossRef]
59. Xu, Y.; Gao, T.; Liang, Y.; Xiao, D. Intercalation Lithium Cobalt Oxide for the Facile Fabrication of a Sensitive Dopamine Sensor. *ChemElectroChem* **2020**, *7*, 1193–1200. [CrossRef]

60. Manbohi, A.; Ahmadi, S.H. Sensitive and selective detection of dopamine using electrochemical microfluidic paper-based analytical nanosensor. *Sens. Bio-Sens. Res.* **2019**, *23*, 100270. [CrossRef]
61. da Silva, V.N.C.; Farias, E.A.D.O.; Araújo, A.R.; Magalhães, F.E.X.; Fernandes, J.R.N.; Souza, J.M.T.; Eiras, C.; da Silva, D.A.; Bastos, V.H.D.V.; Teixeira, S.S. Rapid and selective detection of dopamine in human serum using an electrochemical sensor based on zinc oxide nanoparticles, nickel phthalocyanines, and carbon nanotubes. *Biosens. Bioelectron.* **2022**, *210*, 114211. [CrossRef]
62. Gong, Q.; Han, H.; Wang, Y.; Yao, C.; Yang, H.; Qiao, J. An electrochemical sensor for dopamine detection based on the electrode of a poly-tryptophan-functionalized graphene composite. *New Carbon Mater.* **2020**, *35*, 34–41. [CrossRef]
63. Arumugasamy, S.K.; Govindaraju, S.; Yun, K. Electrochemical sensor for detecting dopamine using graphene quantum dots incorporated with multiwall carbon nanotubes. *Appl. Surf. Sci.* **2020**, *508*, 145294. [CrossRef]
64. Pang, P.; Yan, F.; Li, H.; Li, H.; Zhang, Y.; Wang, H.; Wu, Z.; Yang, W. Graphene quantum dots and Nafion composite as an ultrasensitive electrochemical sensor for the detection of dopamine. *Anal. Methods* **2016**, *8*, 4912–4918. [CrossRef]
65. Huang, Q.; Lin, X.; Tong, L.; Tong, Q.-X. Graphene Quantum Dots/Multiwalled Carbon Nanotubes Composite-Based Electrochemical Sensor for Detecting Dopamine Release from Living Cells. *ACS Sustain. Chem. Eng.* **2020**, *8*, 1644–1650. [CrossRef]
66. Beitollahi, H.; Dourandish, Z.; Ganjali, M.R.; Shakeri, S. Voltammetric determination of dopamine in the presence of tyrosine using graphite screen-printed electrode modified with graphene quantum dots. *Ionics* **2018**, *24*, 4023–4031. [CrossRef]
67. Ben Aoun, S. Nanostructured carbon electrode modified with N-doped graphene quantum dots–chitosan nanocomposite: A sensitive electrochemical dopamine sensor. *R. Soc. Open Sci.* **2017**, *4*, 171199. [CrossRef]

Disclaimer/Publisher's Note: The statements, opinions and data contained in all publications are solely those of the individual author(s) and contributor(s) and not of MDPI and/or the editor(s). MDPI and/or the editor(s) disclaim responsibility for any injury to people or property resulting from any ideas, methods, instructions or products referred to in the content.